2016 American Control Conference (ACC)
Boston Marriott Copley Place
July 6-8, 2016. Boston, MA, USA

Black-Box Modeling of Connected Vehicle Networks

Linjun Zhang and Gábor Orosz

***Abstract*— In this paper, we propose a black-box modeling framework for connected vehicle networks comprised of conventional vehicles and vehicles equipped with wireless vehicle-to-vehicle (V2V) communication. First, we identify the link length that is the number of vehicles between the broadcasting and the host vehicle. Based on the estimated link length, a linear model is used to approximate the dynamics of the vehicle network. The proposed framework does not require priori information about the dynamics of the vehicle network, and hence can be implemented in real traffic. Numerical simulations are used to demonstrate the effectiveness of the estimators in capturing the link length and predicting the time evolution of the vehicle network. The estimated model can be used when designing connected cruise control (CCC) algorithms.**

I. INTRODUCTION

In recent years, exploiting wireless vehicle-to-vehicle (V2V) communication in vehicle control systems has been receiving increasing attention. With the capability of monitoring distant vehicles beyond the line of sight, V2V communication has potentials in improving traffic mobility, enhancing vehicle safety, and reducing fuel consumption.

One common way to apply V2V communication is to construct cooperative adaptive cruise control (CACC), which is a vehicle platoon where all vehicles automatically respond to the vehicle immediately ahead relying on range sensors (e.g, radar) while also responding to the motion of a designated platoon leader [1]–[5]. There are two restrictions of CACC that limit its implementation in real traffic. On one hand, it requires that autonomous vehicles travel next to each other to form a platoon, which rarely occurs in practice due to the low penetration of such vehicles. On the other hand, it requires that all following vehicles communicate with a designated platoon leader, which restricts the connectivity topology. To relax these limitations, connected cruise control (CCC) was proposed [6], [7], which allows the incorporation of human-driven vehicles that may be not equipped with communication devices. Moreover, CCC requires neither a designated leader nor a prescribed connectivity structure. The flexibility of CCC makes it practical to implement in real traffic.

When designing CCC for system-level properties such as string stability [2] and collision avoidance [8], one needs to know the dynamics of the vehicle network, which is indeed unavailable in practice. In [9], the authors used the intelligent driver model (IDM) to predict the response of the vehicle immediately ahead. However, they assumed that the number of vehicles between the broadcasting and the host vehicle was known while all vehicles could be described by the same model. The main contribution of this paper is an estimator framework that allows one to identify the dynamics of vehicle networks without requiring any prior knowledge about the system. We first provide a link length estimator to identify the number of vehicles between the broadcasting and the host vehicle. This determines the number of states in the dynamics. Then, we use a discrete-time linear model to approximate the dynamics, where the coefficients are determined by minimizing a cost function. Numerical simulations are used to show the effectiveness of the proposed estimator in identifying the link length and predicting the network behavior.

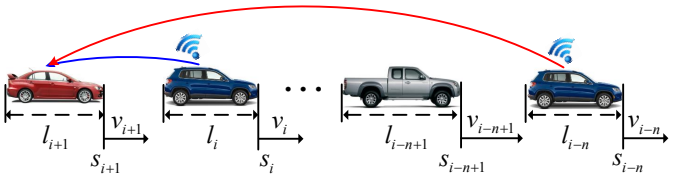

Fig. 1. Vehicle network where a CCC vehicle (red) receives information from multiple vehicles ahead. Symbols s_j, l_j and v_j denote the position, length and velocity of vehicle j, respectively. The blue link can be realized by human perception, range sensors, and V2V communication while the red link can only be realized by V2V communication. Notice that vehicle $i-n+1$ does not broadcast its information.

II. LINK LENGTH ESTIMATOR

In this section, we present the link length estimator (LLE) to identify the number of vehicles between the broadcasting and the host vehicle by using position and velocity information received via V2V communication. In Fig. 1, vehicle $i+1$ (red) monitors the positions s_j and the velocities v_j of some vehicles among vehicles $i,\dots,i-n$ within the effective communication range. We emphasize that the vehicle network may include vehicles that do not broadcast information (e.g., vehicle $i-n+1$ in Fig. 1). The symbol l_j represents the length of vehicle j. The vehicle immediately ahead can be monitored by human perception, by range sensors (e.g., radar), or by V2V communication while distant vehicles can only be monitored by using V2V communication since they are out of the line of sight.

We use the word "headway" to describe the bumper-to-bumper distance between two consecutive vehicles so that the average headway $h_{i,j}$ between vehicle i and vehicle j

The authors are both with the Department of Mechanical Engineering, University of Michigan, Ann Arbor, MI, 48109, USA linjunzh@umich.edu, orosz@umich.edu

This work was supported by the National Science Foundation (Award Number 1351456).

($j<i$) can be expressed by

$$h_{i,j}=\frac{s_j-s_i-\sum_{k=j}^{i-1}l_k}{i-j}, \tag{1}$$

see Fig. 1.

Let $v_{j,\max}$ denote the admissible maximum velocity of vehicle j, which is determined by traffic laws or by the driver's intention. Traffic data show that, when vehicles $j-1$ and j move at a constant speed $0<v^*<v_{j,\max}$, vehicle j aims to keep a constant speed-dependent headway $h^*_{j,j-1}$ [10]. This relationship is called *range policy* that can be described by the function

$$h^*_{j,j-1}=s^*_{j-1}-s^*_j-l_{j-1}=H_j(v^*). \tag{2}$$

Here, the function $H_j(v^*)>0$ is continuous and monotonically increasing with v^*. Note that when $v^*=0$ vehicle j can maintain the headway $0<h^*_{j,j-1}\le H_j(0)$ while $v^*=v_{j,\max}$ results in $h^*_{j,j-1}\ge H_j(v_{j,\max})$.

When all vehicles move at the same constant velocity v^* and they all use the same range policy $H(v^*)$, we obtain the *uniform flow equilibrium*,

$$h^*_{j,j-1}=h^*=H(v^*), \tag{3}$$

for all $j=i-n,\dots,i+1$; cf. (1) and (2). In real traffic, range policies may vary among different drivers in which case the equilibrium still exists but is not uniform, i.e., $h^*_{j,j-1}\neq h^*_{k,k-1}$ for $j\neq k$; see (2). In this situation, the average equilibrium headway between vehicles i and j is given by

$$h^*_{i,j}=\frac{s^*_j-s^*_i-(i-j)l_{\rm av}}{i-j}=H_{\rm av}(v^*), \tag{4}$$

where the average vehicle length $l_{\rm av}$ and the average range policy $H_{\rm av}(v^*)$ are given by

$$l_{\rm av}=\frac{1}{i-j}\sum_{k=j}^{i-1}l_k,\quad H_{\rm av}(v^*)=\frac{1}{i-j}\sum_{k=j+1}^{i}H_k(v^*). \tag{5}$$

Note that the length of vehicle i and the range policy of vehicle j are not included in (4); cf. (1)–(3).

Then, we present the LLE that can estimate the number of vehicles between any pair of communicating vehicles. Here, we are interested in the link length between vehicles i and $i-n$, which is the total number of vehicles in the communication range of the CCC vehicle $i+1$. According to (4), we have

$$n=\frac{s^*_{i-n}-s^*_i}{l_{\rm av}+H_{\rm av}(v^*)}. \tag{6}$$

In practice, the information about $l_{\rm av}$ and $H_{\rm av}(v^*)$ in (6) are not available when there exist vehicles that do not broadcast information. Thus, in practice, we use the approximations

$$\bar{l}_{\rm av}\approx l_{\rm av},\quad \overline{H}_{\rm av}(v^*)\approx H_{\rm av}(v^*), \tag{7}$$

which may be generated by statistical analysis of empirical traffic data.

In real traffic, the equilibrium information s^*_k and v^* cannot be obtained directly. According to the UMTRI Safety Pilot experiment [11], V2V communication provides data intermittently with sampling time $\Delta t=0.1$ [s]. Suppose that at the time instant $t_k=k\Delta t$, vehicle $i+1$ receives position and velocity data $s_i(t_k)$, $v_i(t_k)$, $s_{i-n}(t_k)$, $v_{i-n}(t_k)$ from vehicles i and $i-n$. Assuming that the traffic flow is around the equilibrium, we define the averages

$$\begin{aligned}
\xi_1(t_k)&\triangleq\mathbb{E}^{t_k}_{t_0}\big[s_{i-n}(t_j)-s_i(t_j)\big],\\
\xi_2(t_k)&\triangleq\mathbb{E}^{t_k}_{t_0}\big[v_{i-n}(t_j)\big],\\
\xi_3(t_k)&\triangleq\mathbb{E}^{t_k}_{t_0}\left[\frac{\xi_1(t_j)}{\bar{l}_{\rm av}+\overline{H}_{\rm av}(\xi_2(t_j))}\right]
\end{aligned} \tag{8}$$

for the distance, velocity, and link length, respectively, where $\mathbb{E}^{t_k}_{t_0}\big[x(t_j)\big]\triangleq\sum_{j=0}^{k}x(t_j)/(k+1)$. When the perturbation about the equilibrium has zero mean, we have $\xi_1(t_k)\to s^*_{i-n}-s^*_i$ and $\xi_2(t_k)\to v^*$ as $t\to\infty$.

Rewriting (8) in the iterative form and defining $\hat{n}(t_k)$ as the output, we propose the LLE as follow.

$$\begin{aligned}
\xi_1(t_k)&=\xi_1(t_{k-1})+\frac{s_{i-n}(t_k)-s_i(t_k)-\xi_1(t_{k-1})}{k},\\
\xi_2(t_k)&=\xi_2(t_{k-1})+\frac{v_{i-n}(t_k)-\xi_2(t_{k-1})}{k},\\
\xi_3(t_k)&=\xi_3(t_{k-1})+\frac{1}{k}\Big(\frac{\xi_1(t_k)}{\bar{l}_{\rm av}+\overline{H}_{\rm av}\big(\xi_2(t_k)\big)}-\xi_3(t_{k-1})\Big),\\
\hat{n}(t_k)&=\mathrm{int}\big(\xi_3(t_k)\big),
\end{aligned} \tag{9}$$

for $k=1,2,\dots$, where the operation $\mathrm{int}(\xi_3)$ rounds ξ_3 to the nearest integer since the link length must be an integer. Here, the initial conditions are set as $\xi_1(t_0)=\xi_2(t_0)=\xi_3(t_0)=0$.

Theorem 1: Suppose that the measurement errors in position s and velocity v have zero mean. Then, the LLE (9) converges to the actual link length, i.e., $\hat{n}(t_k)\to n$ as $k\to\infty$, if and only if the following condition holds:

$$1-\frac{0.5}{n}<\frac{l_{\rm av}+H_{\rm av}(v^*)}{\bar{l}_{\rm av}+\overline{H}_{\rm av}(v^*)}<1+\frac{0.5}{n}. \tag{10}$$

The proof is given in Appendix A. Indeed, Theorem 1 shows that, as the link length n increases, the convergence of LLE (9) requires higher accuracy of the approximated average vehicle length $\bar{l}_{\rm av}$ and the approximated average range policy $\overline{H}_{\rm av}(v^*)$. The accuracy of such information can be improved when more vehicles broadcast information. However, we remark that LLE (9) does not rely on the motion data of vehicles $i-1,\dots,i-n+1$ so that LLE can be also applied when they do not broadcast.

III. Network Dynamics Identifier

To design CCC for vehicle $i+1$ that satisfies system-level requirements such as string stability, it is necessary to identify the dynamics of the network; see Fig. 1 containing vehicles $i-n,\dots,i$. To achieve this goal, we present the network dynamics identifier (NDI) in this section. We begin by defining the state of this vehicle network as

$$X=[s_{i-n},v_{i-n},\dots,s_i,v_i]^{\rm T}. \tag{11}$$

Here, we neglect the information delays that may arise from human reaction, digital processing, or intermittency

and packet drops in wireless communication. Then, the car-following dynamics of the vehicle network can be described by an ordinary differential equation

$$\dot{X} = f(X, v_{i-n}). \tag{12}$$

Here, we consider v_{i-n} and v_i as the input and the output of the network, respectively, since the speed variation of vehicle $i-n$ propagates through the whole network and eventually affects the speed of vehicle i. In real traffic, the function f is nonlinear.

For CCC design, we need to estimate the input-output dynamics of (12). Although a nonlinear model may improve the estimation accuracy, it will increase the complexity for the subsequent CCC design. Considering that stable nonlinear systems can be approximated by linear systems with bounded errors, we use a linear discrete-time model

$$\hat{v}_i(t_k) = \sum_{q=1}^{N} a_q \hat{v}_i(t_{k-q}) + b_q v_{i-n}(t_{k-q}) = \theta^{\mathrm{T}} \varphi \tag{13}$$

to approximate the input-output dynamics of the nonlinear network (12), where the coefficients and the regressor are given by

$$\theta = \begin{bmatrix} a_1 \\ \vdots \\ a_N \\ b_1 \\ \vdots \\ b_N \end{bmatrix}, \quad \varphi = \begin{bmatrix} \hat{v}_i(t_{k-1}) \\ \vdots \\ \hat{v}_i(t_{k-N}) \\ v_{i-n}(t_{k-1}) \\ \vdots \\ v_{i-n}(t_{k-N}) \end{bmatrix}, \tag{14}$$

respectively. Note that the regressor φ is comprised of measured states and estimated states while the coefficient vector θ and the regression length N are to be determined.

Neglecting information delays, we can write the car-following dynamics of vehicle j in the form

$$\begin{bmatrix} \dot{s}_j \\ \dot{v}_j \end{bmatrix} = \begin{bmatrix} 0 & 1 \\ 0 & 0 \end{bmatrix} \begin{bmatrix} s_j \\ v_j \end{bmatrix} + \begin{bmatrix} 0 \\ 1 \end{bmatrix} u_j, \tag{15}$$

where u_j denotes the acceleration input. Discretizing this model leads to a second order discrete-time model. Thus, for a n-vehicle network, we set the regression length as $N = 2n$. Since n is typically unknown in practice, we use $N = 2\hat{n}$ instead where $\hat{n}$ is the estimated number of vehicles in the network given by LLE (9). Note that $\hat{n}$ must maintain unchanged when identifying the coefficients in θ. The change of $\hat{n}$ indicates that the network size may have changed due to the cut-in and/or the cut-off of vehicles so that the dynamics of the vehicle network changes as well. In this case, the NDI must be restarted with the corresponding N.

In (13), the value of θ can be determined by minimizing the error between the measured output v_i and the estimated output $\hat{v}_i$ of the vehicle network, that is, we determine θ by minimizing the cost function

$$J = \sum_{k=r}^{r+\delta} \left(v_i(t_k) - \hat{v}_i(t_k) \right)^2, \tag{16}$$

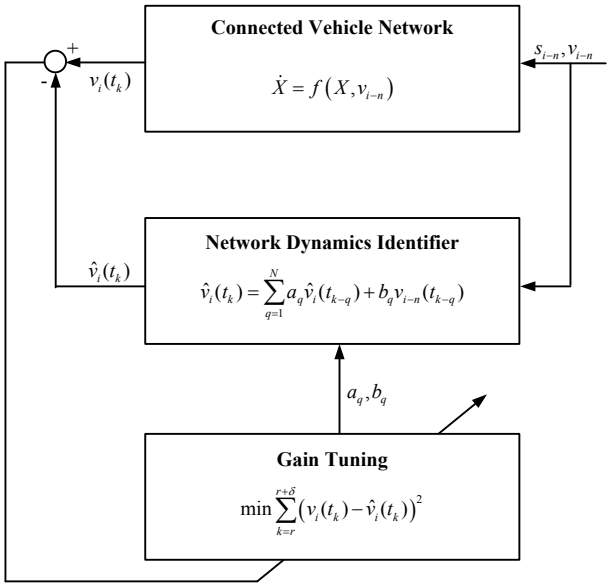

Fig. 2. Information flow diagram of network dynamics identifier.

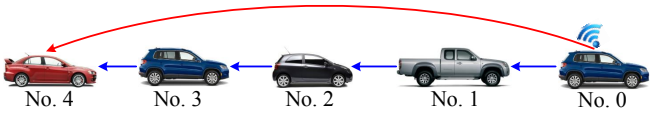

Fig. 3. A vehicle network where vehicle 4 monitors vehicle 3 and vehicle 0 while other vehicles only responds to the motion of the vehicle immediately ahead.

where $r, \delta \in \mathbb{N}$. Note that $t_r = r\Delta t$ and $t_\delta = \delta \Delta t$ denote the start time and the window size of the data for training the NDI to estimate θ. Typically, the estimation accuracy increases with the window size t_δ, but this also increases the computational cost. To solve the minimization of (16) subject to the dynamics (13), we utilize the differential evolution (DE) approach [12], which maintains a population of candidate solutions and iteratively improves these candidate solutions in terms of their costs. A brief description of the DE approach is given in Appendix B. We remark that one may use other approaches to solve the optimization problem. Here, we use DE since it does not require gradient information, which simplifies its application.

Given sufficiently large number of iterations, DE can lead to the global minimum. However, to achieve real-time estimation in practice, the maximum number of iterations is limited by the on-board computational resources so that the result may end up in the vicinity of a local minimum. After reaching the maximum number of iterations, the DE computation yields the coefficients a_q, b_q for $q = 1, \ldots, N$, which are left unchanged for predicting the behavior of the vehicle network and for the subsequent CCC design. The information flow of NDI is summarized in Fig. 2.

IV. Numerical Simulations

In this section, we consider a 5-vehicle network shown in Fig. 3, where the CCC vehicle 4 monitors the motion of

vehicle 0 and vehicle 3 while other vehicles only respond to the motion of the vehicle immediately ahead. Here, we assume that vehicle 4 is driven by a human driver and test the performance of the estimators presented in Sections II and III.

To simulate the heterogeneity of vehicles, we use different models and parameters for different vehicles. Specifically, we use the optimal velocity model (OVM) [10] for vehicles 1 and 3, that is,

$$\begin{aligned} \dot{s}_j &= v_j\,, \\ \dot{v}_j &= \alpha_j\big(V_j(h_{j,j-1}) - v_j\big) + \beta_j(W_j(v_{j-1}) - v_j)\,, \end{aligned} \tag{17}$$

for $j = 1,3$. Here, the constants α_j and β_j are control gains for headway and relative velocity, respectively, and the functions $V_j(h)$ and $W_j(v)$ are given by

$$V_j(h) = \begin{cases} 0\,, & \text{if } h \le h_{j,\mathrm{st}}\,, \\ \frac{v_{j,\max}}{2}\left[1 - \cos\left(\pi \frac{h - h_{j,\mathrm{st}}}{h_{j,\mathrm{go}} - h_{j,\mathrm{st}}}\right)\right], & \text{if } h_{j,\mathrm{st}} < h < h_{j,\mathrm{go}}\,, \\ v_{j,\max}\,, & \text{if } h \ge h_{j,\mathrm{go}}\,, \end{cases}$$

$$W_j(v) = \begin{cases} v\,, & \text{if } v \le v_{j,\max}\,, \\ v_{j,\max}\,, & \text{if } v > v_{j,\max}\,. \end{cases} \tag{18}$$

The function $V_j(h)$ indicates that the vehicle tends to stop when the headway is small while aiming to maintain the admissible maximum velocity $v_{j,\max}$ for large headways. Between $h_{j,\mathrm{st}}$ and $h_{j,\mathrm{go}}$, the nonlinear and monotonically increasing function is selected such that derivatives at $h = h_{j,\mathrm{st}}$ and $h = h_{j,\mathrm{go}}$ are smooth, yielding smooth change of acceleration that is important for driving comfort. The saturation function $W_j(v)$ ensures that vehicle j does not try to follow the vehicle immediately ahead when $v_{j-1} > v_{j,\max}$.

For vehicles 2 and 4, we use the intelligent driver model (IDM) [13] given by

$$\begin{aligned} \dot{s}_j &= v_j\,, \\ \dot{v}_j &= a_j\left[1 - \left(\frac{v_j}{v_{j,\max}}\right)^4 - \left(\frac{g(v_j, v_{j-1})}{h_{j,j-1}}\right)^2\right], \end{aligned} \tag{19}$$

for $j = 2,4$, where

$$g(v_j, v_{j-1}) = h_{j,\mathrm{st}} + v_j T_j + \frac{v_j(v_j - v_{j-1})}{2\sqrt{a_j b_j}}\,. \tag{20}$$

Here, parameters a_j and b_j represent the desired maximum acceleration and deceleration, respectively, while T_j denotes the desired time gap.

When all vehicles move at the same velocity v^*, we obtain the range policies

$$\begin{aligned} H_{\mathrm{OVM}}(v^*) &= h_{j,\mathrm{st}} + \frac{h_{j,\mathrm{go}} - h_{j,\mathrm{st}}}{\pi} \arccos\left(1 - \frac{2v^*}{v_{j,\max}}\right), \\ H_{\mathrm{IDM}}(v^*) &= \frac{h_{j,\mathrm{st}} + v^* T_j}{\sqrt{1 - (v^*/v_{j,\max})^4}}\,, \end{aligned} \tag{21}$$

see Fig. 5(a). It can be seen that for $0 < v^* < v_{j,\max}$, $H_j(v^*)$ is continuous and monotonically increasing. The equilibrium

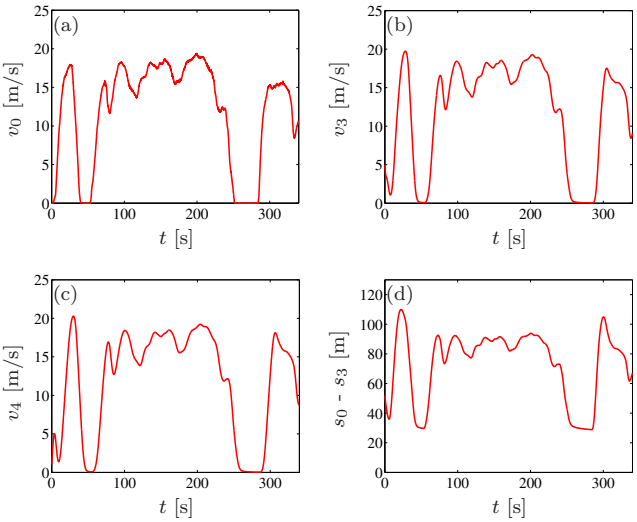

Fig. 4. (a) Reference velocity of vehicle 0, which is obtained from UMTRI's Safety Pilot project. (b,c) Velocities of vehicles 3 and 4. (d) Distance between vehicle 3 and vehicle 0.

headway for $v^* = 0$ is $0 < h^*_{j,j-1} \le H_j(0) = h_{j,\mathrm{st}}$, while for $v^* \ge v_{j,\max}$ we have $h^*_{j,j-1} \ge H_j(v_{j,\max}) = h_{j,\mathrm{go}}$

To simulate the vehicle network, we use the experimental data from UMTRI Safe Pilot [11] for the head vehicle 0, which is shown by the red solid curve in Fig. 4(a). Note that the measured data is in discrete time with sampling rate $\Delta t = 0.1$ [s]. Here we apply the linear interpolation to the experimental data and obtain a continuous trajectory. The motion of other vehicles is governed by the OVM (17) or the IDM (19) with the following parameters.

- Vehicle 1 is modeled by OVM with $\alpha_1 = 0.6$ [1/s], $\beta_1 = 0.7$ [1/s], $h_{\mathrm{st},1} = 5$ [m], $h_{\mathrm{go},1} = 35$ [m], $v_{\max,1} = 30$ [m/s].
- Vehicle 2 is modeled by IDM with $a_2 = 1.3$ [m/s^2], $b_2 = 2$ [m/s^2], $h_{\mathrm{st},2} = 2.5$ [m], $T_2 = 1.5$ [s], $v_{\max,2} = 43$ [m/s].
- Vehicle 3 is modeled by OVM with $\alpha_3 = 0.4$ [1/s], $\beta_3 = 0.5$ [1/s], $h_{\mathrm{st},3} = 6$ [m], $h_{\mathrm{go},3} = 40$ [m], $v_{\max,3} = 33$ [m/s].
- Vehicle 4 is modeled by IDM with $a_4 = 1.6$ [m/s^2], $b_4 = 2$ [m/s^2], $h_{\mathrm{st},4} = 2$ [m], $T_4 = 1.3$ [s], $v_{\max,4} = 40$ [m/s].

We also consider different lengths for different vehicles: $l_0 = 4.8$ [m], $l_1 = 5.5$ [m], $l_2 = 3.6$ [m], $l_3 = 4.6$ [m], and $l_4 = 4.1$ [m]. To estimate the link length, vehicle 4 calculates the distance between vehicles 0 and 3 that includes the lengths of vehicles 0–2, for which the average vehicle length is $l_{\mathrm{av}} \approx 4.63$ [m]; cf. (5). However, this information cannot be obtained in practice. When using LLE (9), we approximate the average vehicle length by $\bar{l}_{\mathrm{av}} = 4.5$ [m].

The initial positions and velocities of all vehicles are provided as follows: $s_0(0) = 0$ [m], $s_1(0) = -19.8$ [m], $s_2(0) = -35.3$ [m], $s_3(0) = -51.9$ [m], $s_4(0) = -68.5$ [m], $v_0(0) = 0$ [m/s], $v_1(0) = 5$ [m/s], $v_2(0) = 3$ [m/s], $v_3(0) = 5$ [m/s], and $v_4(0) = 1$ [m/s].

The CCC vehicle 4 monitors the positions and velocities of vehicle 0 and vehicle 3 while also calculating the distance

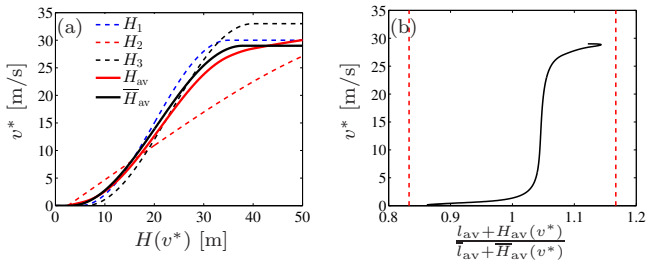

Fig. 5. (a) Range policies $H_j(v^*)$ of vehicles $j=1$–3 (dashed), the average range policy $H_{\rm av}(v^*)$ (red solid), and the approximated average range policy $\overline{H}_{\rm av}(v^*)$ (black solid). (b) Ratio (10) between the average values and their approximated values.

between vehicles 0 and 3, as shown in Fig. 4. Then, we apply the LLE (9) to estimate the network size. Range policies (21) for vehicles 1–3 are shown in Fig. 5(a) by dashed curves. The solid red curve displays the average of range policy $H_{\rm av}(v^*)$ for vehicles 1–3; cf. (5). Since in practice $H_{\rm av}(v^*)$ is not available, we use the approximated average range policy in the OVM form, i.e., $\overline{H}_{\rm av}(v^*)=H_{\rm OVM}(v^*)$, and set the parameters as $h_{\rm st}=3$ [m], $h_{\rm go}=38$ [m], and $v_{\max}=29$ [m/s]; cf. (21). The ratio $\frac{l_{\rm av}+H_{\rm av}(v^*)}{l_{\rm av}+\overline{H}_{\rm av}(v^*)}$ used in Theorem 1 is plotted in Fig. 5(b). The link length between vehicles 0 and 3 is $n=3$. Hence, according to (10), the convergence of $\hat{n}(t_k)$ to n can be guaranteed if $0.833 \le \frac{l_{\rm av}+H_{\rm av}(v^*)}{l_{\rm av}+\overline{H}_{\rm av}(v^*)} \le 1.167$ that is between the two red vertical lines in Fig. 5(b). Based on our chosen average values, the convergence is always guaranteed.

In the cost function (13), we set the window size as $t_\delta=30$ [s]. Parameters for DE computation are set as follows: population $N_{\rm p}=30$, maximum generation $g_{\max}=200$, mutation factor $F=0.9$, and crossover factor $Cr=0.8$. Then, we use the LLE (9) and the NDI (13) to estimate the network size and the network dynamics, respectively. The results are shown in Fig. 6, where panel (a) shows that the estimated network size $\hat{n}$ (dashed line) converges to the actual network size n (solid line). After $t_r=51.8$ [s], $\hat{n}=3$ is unchanged for $t_\delta=30$ [s]. Therefore, the data between $t_r=51.8$ [s] and $t_r+t_\delta=81.8$ [s] are utilized for training the NDI to identify the dynamics of the network. When the DE computation reaches the preset maximum generation $g_{\max}=200$, the coefficients in (13) are obtained as given in Table I. The evolution of cost (16) is shown in Fig. 6(b), which decreases along iterations. Note that the identified values in Table I are left unchanged since $\hat{n}$ does not change. Then, by using these coefficients and using the data in the time domain 51.8–81.8 [s] as initial condition, we simulate the the linear discrete-time model (13) as shown by the dashed-dotted black curve in Fig. 6(c) with the tracking errors given in Fig. 6(d). These results demonstrate that the obtained model can reproduce the dynamics of the vehicle network.

V. Conclusions

In this paper, we proposed a black-box modeling framework for connected vehicle networks, which can be used in the design of connected cruise control. First, we presented

TABLE I

Identified values for a_1–a_6 and b_1–b_6 using the NDI (13).

a_1	-0.5587	b_1	-0.9536
a_2	-0.0059	b_2	-1.2371
a_3	0.4807	b_3	2.0490
a_4	0.4245	b_4	0.4873
a_5	0.1410	b_5	0.7339
a_6	0.3635	b_6	-0.9178

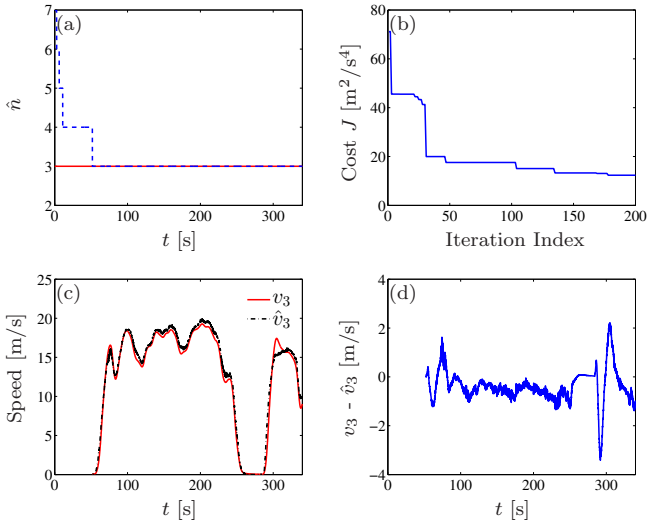

Fig. 6. (a) Estimation of network size. (b) Evolution of cost functions (16) based on DE computation. (c) Actual velocity (red solid) and estimated velocity (black dashed-dotted) of vehicle 3. (d) Error between the actual velocity v_3 and the estimated velocity $\hat{v}_3$.

an link length estimator to identify the number of vehicles in the network, which determined the number of states in the network. Then, a linear discrete-time model was used to approximate the dynamics of nonlinear vehicle networks, where the coefficients in the model were obtained by minimizing an error function. Numerical simulations were used to validate the analytical results and show that the estimated model can predict the behavior of vehicle networks. Therefore, our presented estimator could be used in the design of connected cruise control.

In practice, there exist packet drops in V2V communication and the road geometry may also be more complex. How to make the presented estimators robust against these effects will be investigated in the future. The integration of the presented estimators in connected cruise control design will be also studied.

Appendix A: Proof of Theorem 1

For a vehicle network, we have

$$\begin{aligned} s_j - s_i &= s_j^* - s_i^* + \tilde{d}_{i,j}\,, \\ v_j &= v^* + \tilde{v}_j\,, \end{aligned} \tag{22}$$

where the uniform flow equilibrium $s_j^*-s_i^* \equiv d_{i,j}^*$ and v^* can be seen as the constant components in the Fourier series of s_j-s_i and v_j while the perturbations $\tilde{d}_{i,j}$ and $\tilde{v}_j$ are composed of all sinusoidal terms of the Fourier series. Note

that measurement errors may also be included in $\tilde{d}_{i,j}$ and $\tilde{v}_j$. It follows that

$$\mathbb{E}_{t_0}^{t_k}\left[\tilde{d}_{i,j}(t_p)\right] \to 0\,, \quad \mathbb{E}_{t_0}^{t_k}\left[\tilde{v}_j(t_p)\right] \to 0\,, \tag{23}$$

as $k \to \infty$.

Substituting (22) and (23) into (8) leads to

$$\begin{aligned} \xi_1(t_k) &\to s^*_{i-n} - s^*_{i-1}\,, \\ \xi_2(t_k) &\to v^*\,, \\ \xi_3(t_k) &\to \frac{s^*_{i-n} - s^*_{i-1}}{\overline{l}_{\mathrm{av}} + \overline{H}_{\mathrm{av}}(v^*)}\,, \end{aligned} \tag{24}$$

as $k \to \infty$. Hence, the steady-state output of LLE (9) becomes

$$\lim_{k\to\infty} \hat{n}(t_k) = \mathrm{int}\left(\frac{s^*_{i-n} - s^*_{i-1}}{\overline{l}_{\mathrm{av}} + \overline{H}_{\mathrm{av}}(v^*)}\right). \tag{25}$$

At the uniform flow, we have

$$s^*_{i-n} - s^*_{i-1} = n\big(l_{\mathrm{av}} + H_{\mathrm{av}}(v^*)\big)\,, \tag{26}$$

cf. (4). Substituting (26) into (25) leads to

$$\lim_{k\to\infty} \hat{n}(t_k) = \mathrm{int}\left(\frac{l_{\mathrm{av}} + H_{\mathrm{av}}(v^*)}{\overline{l}_{\mathrm{av}} + \overline{H}_{\mathrm{av}}(v^*)} n\right). \tag{27}$$

When the condition (10) holds, it follows that

$$n - 0.5 < \frac{l_{\mathrm{av}} + H_{\mathrm{av}}(v^*)}{\overline{l}_{\mathrm{av}} + \overline{H}_{\mathrm{av}}(v^*)} n < n + 0.5\,. \tag{28}$$

Rounding real numbers to the closest integer yields $\lim_{k\to\infty} \hat{n}(t_k) = n$; cf. (27,28).

Appendix B: Procedure of Differential Evolution Approach

A brief introduction of the differential evolution approach is provided as follows.

- Set population $P_g = \left\{\theta_{1,g}, \ldots, \theta_{N_\mathrm{p},g}\right\}$, where g denotes the generation, N_p is the population size, and the vector $\theta_{i,g} \in \mathbb{R}^m$ is a candidate solution for $i = 1, \ldots, N_\mathrm{p}$.
- Randomly initialize the population of generation 0, i.e., P_0, in a prescribed domain.
- Mutation: Recombine the population to produce N_p trial vectors, i.e., $\eta_{i,g} = \theta_{r_0,g} + F(\theta_{r_1,g} - \theta_{r_2,g})$ for $i = 1, \ldots, N_\mathrm{p}$, where r_0, r_1, r_2 are randomly selected from the set $\{1, \ldots, N_\mathrm{p}\}$ and the scalar factor $F > 0$ controls the evolution rate. There is no upper limit on F, but effective value is typically smaller than 1.
- Crossover. DE produces a new vector by crossing each vector with a mutant vector, that is

$$\left[\vartheta_{i,g}\right]_j = \begin{cases} \left[\eta_{i,g}\right]_j, & \text{if } \mathrm{rand}(0,1) \le Cr\,, \\ \left[\theta_{i,g}\right]_j, & \text{otherwise}, \end{cases} \tag{29}$$

  where $\left[\vartheta_{i,g}\right]_j$ denotes the j-th element in the vector $\vartheta_{i,g}$, $\mathrm{rand}(0,1)$ yields a random real value between 0 and 1, and the crossover probability $Cr \in [0,1]$ controls the fraction of values copied from the mutant.
- Select the lower-cost one from the target vector $\theta_{i,g}$ and the mutant $\vartheta_{i,g}$, and then pass it to the next generation. That is,

$$\theta_{i,g+1} = \begin{cases} \vartheta_{i,g}\,, & \text{if } J(\vartheta_{i,g}) \le J(\theta_{i,g})\,, \\ \theta_{i,g}\,, & \text{otherwise}\,. \end{cases} \tag{30}$$

Detailed description of the differential evolution approach is provided in [12].

References

[1] V. Milanés and S. E. Shladover, "Modeling cooperative and autonomous adaptive cruise control dynamic responses using experimental data," *Transportation Research Part C*, vol. 48, pp. 285–300, 2014.

[2] J. Ploeg, D. P. Shukla, N. van de Wouw, and H. Nijmeijer, "Controller synthesis for string stability of vehicle platoons," *IEEE Transactions on Intelligent Transportation Systems*, vol. 15, no. 2, pp. 854–865, 2014.

[3] S. Öncü, J. Ploeg, N. van de Wouw, and H. Nijmeijer, "Cooperative adaptive cruise control: network-aware analysis of string stability," *IEEE Transactions on Intelligent Transportation Systems*, vol. 15, no. 4, pp. 1527–1537, 2014.

[4] A. Alam, J. Mårtensson, and K. H. Johansson, "Experimental evaluation of decentralized cooperative cruise control for heavy-duty vehicle platooning," *Control Engineering Practice*, vol. 38, pp. 11–25, 2015.

[5] R. Kianfar, B. Augusto, A. Ebadighajari, U. Hakeem, J. Nilsson, A. Raza, R. S. Tabar, N. V. Irukulapati, C. Englund, P. Falcone, S. Papanastasiou, L. Svensson, and H. Wymeersch, "Design and experimental validation of a cooperative driving system in the grand cooperative driving challenge," *IEEE Transactions on Intelligent Transportation Systems*, vol. 13, no. 3, pp. 994–1007, 2012.

[6] L. Zhang and G. Orosz, "Motif-based design for connected vehicle systems in presence of heterogeneous connectivity structures and time delays," *IEEE Transactions on Intelligent Transportation Systems*, p. (accepted), 2016.

[7] J. I. Ge and G. Orosz, "Dynamics of connected vehicle systems with delayed acceleration feedback," *Transportation Research Part C*, vol. 46, pp. 46–64, 2014.

[8] A. Alam, A. Gattamin, K. Johansson, and C. Tomlin, "Guaranteeing safety for heavy duty vehicle platooning: Safe set computations and experimental evaluations," *Control Engineering Practice*, vol. 24, pp. 33–41, 2014.

[9] R. Pandita and D. Caveney, "Preceding vehicle state prediction," in *IEEE Intelligent Vehicles Symposium*, Gold Coast, Australia, 2013, pp. 1000–1006.

[10] G. Orosz, R. E. Wilson, and G. Stépán, "Traffic jams: dynamics and control," *Philosophical Transactions of the Royal Society A*, vol. 368, no. 1928, pp. 4455–4479, 2010.

[11] "UMTRI Safety Pilot," http://safetypilot.umtri.umich.edu/.

[12] K. V. Price, R. M. Storn, and J. A. Lampinen, *Differential evolution: A practical approach to global optimization*. Springer, 2005.

[13] A. Kesting and M. Treiber, "Calibrating car-following models by using trajectory data," *Transportation Research Record: Journal of the Transportation Research Board*, vol. 2088, no. 1, pp. 148–156, 2008.